Coulomb potential influence in the attoclock experimental scheme

Zhilei Xiao (肖智磊)[1,2], Wei Quan (全 威)[1,*], Songpo Xu (许松坡)[1,2], Shaogang Yu (余少刚)[1,2], Yanlan Wang (王艳兰)[1], Meng Zhao (赵 猛)[1,2], Mingzheng Wei (魏明政)[1], Yu Zhou (周 宇)[1,2], Xuanyang Lai (赖炫扬)[1], Jing Chen (陈 京)[3,4,], and Xiaojun Liu (柳晓军)[1,***]**

[1]*State Key Laboratory of Magnetic Resonance and Atomic and Molecular Physics, Wuhan Institute of Physics and Mathematics, Innovation Academy for Precision Measurement Science and Technology, Chinese Academy of Sciences, Wuhan 430071, China*

[2]*University of Chinese Academy of Sciences, Beijing 100049, China*

[3]*HEDPS, Center for Applied Physics and Technology, Peking University, Beijing 100084, China*

[4]*Institute of Applied Physics and Computational Mathematics, Beijing 100088, China*

**Corresponding author: charlywing@wipm.ac.cn; **corresponding author: chen_jing@iapcm.ac.cn; ***corresponding author: xjliu@wipm.ac.cn*

Received August 24, 2019; accepted September 25, 2019; posted online December 11, 2019

Coulomb potential may induce a significant angular offset to the two-dimensional photoelectron momentum distributions for atoms subject to strong elliptically polarized laser fields. In the attoclock experiment, this offset usually cannot be easily disentangled from the contribution of tunneling delay and poses a main obstacle to the precise measurement of tunneling delay. Based on semiclassical calculations, here, we propose a method to extract the equivalent temporal offset induced solely by Coulomb potential (TOCP) in an attoclock experiment. Our calculations indicate that, at constant laser intensity, the TOCP shows distinctive wavelength dependence laws for different model atoms, and the ratio of the target atom's TOCP to that of H becomes insensitive to wavelength and linearly proportional to $(2I_p)^{-3/2}$, where I_p is the ionization potential of the target atom. This wavelength and I_p dependence of TOCP can be further applied to extract the Coulomb potential influence. Our work paves the way for an accurate measurement of the tunneling delay in the tunneling ionization of atoms subject to intense elliptically polarized laser fields.

Keywords: tunneling delay; Coulomb potential influence; attoclock.
doi: 10.3788/COL202018.010201.

The ultrafast dynamics of atoms and molecules subject to intense laser fields have attracted a lot of attention (see, e.g., Refs. [1–7]). One of the most attractive issues in this field is the tunneling delay problem, i.e., the problem of whether tunneling of a particle through a barrier takes a finite time, which has already been debated for 80 years[3]. The resolution of this problem is paramount to comprehend the tunneling process itself, which is one of the fundamental topics in quantum mechanics. Several experimental procedures with temporal resolution in the scale of attoseconds have been demonstrated to be useful to measure the tunneling delay, such as attosecond streaking[4,5], reconstruction of attosecond beating by interference of two-photon transitions[6,7], and attoclock[8,9].

Among all the experimental schemes mentioned above, attoclock[8,9] is the most intriguing one. This method relies on the relationship between the tunneling time and the rotating electric field vector of a strong elliptically polarized (EP) laser field. Specifically, for atoms subject to the EP laser field, the instant when the electron appears in the continuum is mapped to the final angle of the momentum vector in the polarization plane, which can be measured experimentally. Based on the physical picture of the simpleman model[10,11], the temporal resolution of an attoclock can be determined by the angular frequency of the laser field and also the angular momentum resolution of the spectrometer employed, which may give rise to the temporal resolution in the scale of attoseconds, even for the routinely available femtosecond laser pulses. As well accepted, compared to others, the most crucial advantage of the attoclock scheme is that the attosecond pulse is not necessary any longer, which lowers the technical demand to a great extent and makes this experimental procedure attractive.

On the other hand, the predictions of the simpleman model cannot match the measurements well, because the total ignorance of the Coulomb potential is not operative in the attoclock experiments. In a strong EP laser field, if both the tunneling delay and the Coulomb potential effect are included, a significant rotation offset of the calculated photoelectron momentum distribution (PMD) can be identified compared to the results with only tunneling delay influence considered. That is to say, the Coulomb potential will induce an angular offset of the calculated PMD, which is equivalent to a temporal offset in the attoclock scheme. Moreover, the equivalent temporal offset solely induced by the Coulomb potential (TOCP) could be even larger than the one from the tunneling delay (see, e.g., Ref. [9]). Unfortunately, until now, TOCP can

only be determined from the numerical estimation based on some approximations. However, it is very difficult to accurately calculate the TOCP because some key elements, such as precise value of tunnel exit[12,13], and the initial momentum distributions of photoelectron at the tunneling exit[14–16], are also under hot debate. Therefore, as one may expect, the reliability and temporal resolution of an attoclock are limited, which may hinder the investigation of the issue of tunneling delay.

In fact, the consensus on whether there is a finite tunneling delay has not been achieved so far. In 2008, based on the attoclock experimental results, Eckle *et al.*[9] placed an upper limit of 34 as and an intensity-averaged upper limit of 12 as on the tunneling delay in strong field ionization of He. Several years later, Pfeiffer *et al.*[17] confirmed vanishing tunneling delay time and demonstrated the importance of inclusion of Stark shifts and multi-electron effects. In 2015, Torlina *et al.*[18] employed an *ab initio* numerical simulation method to numerically explore the H atom subject to strong EP laser field with the attoclock scheme, where optical tunneling of the valence electron of a H atom is demonstrated to be instantaneous. With the attoclock technique, a recent experiment on the H atom by Sainadh *et al.*[19] has confirmed the argument for instantaneous tunneling and identified the Coulomb potential as the sole cause of the measured offset angle. As discussed above, some works show that the tunneling process is instantaneous, and no tunneling delay can be revealed. In contrast, a finite tunneling delay has been identified by other groups. In 2014, the refined attoclock measurements of Landsman *et al.*[20] indicated a clear tunneling delay time for a large intensity range. Moreover, recently, in an experimental work of Camus *et al.*[21], a nonzero tunneling time delay has been presented by comparing the PMDs of Ar and Kr under identical experimental conditions. As discussed above, the issue of tunneling delay is still an open question[22–26].

In this Letter, based on the semiclassical calculations, a method is proposed to extract the TOCP in the attoclock scheme, which could be significant to improve the resolution of the attoclock and meaningful to solve the problem of tunneling delay. Our procedure relies on the systematical measurements of two-dimensional PMDs of the target noble gas atoms subject to strong EP laser field at a series of wavelengths for a fixed intensity. According to our calculations, the TOCP depends sensitively on the laser wavelength, especially in the regime of short wavelength, while the ratio of the target atom's TOCP to that of H becomes insensitive to wavelength and linearly proportional to $(2I_p)^{-3/2}$, where I_p is the ionization potential of the atom in question. Therefore, the deviation of TOCP induced by the target atom can be obtained by comparing the wavelength dependence of the TOCP to that of the H atom, for which the TOCP can be measured experimentally or calculated numerically with high accuracy. Note that atomic units ($\hbar = m_e = e = 1$) are used throughout unless otherwise stated.

To explore the Coulomb potential effect on the ultrafast dynamics of atoms subject to strong EP laser field, two numerical methods are applied in our work. Firstly, the basic idea of our procedure is demonstrated with the simpleman model, where Coulomb potential is totally ignored. Secondly, to investigate the influence of Coulomb potential, we further employ the semiclassical methods, where the three-dimensional photoelectron trajectories can be calculated and analyzed.

The simpleman method applied in this work closely follows the ones in the pioneer works[11,27]. The strong field ionization process in an EP pulse can be split in two distinct steps: firstly, the valence electron is injected into the continuum at time t_0 from the origin. Secondly, the free electron propagates in the laser field, and the binding potential is neglected. Here, we let the initial velocity of the electron be zero, and the weight of each electron trajectory is determined by the Ammosov–Delone–Krainov (ADK) theory[28]. To simulate an ionization delay time of Δt, the electron will stay at the origin until $t_0 + \Delta t$, when it is released.

In the semiclassical calculation, we consider a target atom with a H-like potential of

$$V = -\frac{Z_{\text{eff}}}{r}, \tag{1}$$

where $Z_{\text{eff}} = \sqrt{2I_p}$ is the effective nuclear charge, and r denotes the distance between the tunneled electron and the parent ionic core[29]. It is assumed that the electron is released from a bound state to a continuum through tunneling[28,30], and the following dynamics of the tunnel ionized electron is described by a classical Newtonian equation[29,31–35]:

$$\frac{\partial^2 \mathbf{r}}{\partial t^2} = -\mathbf{E}(t) - \nabla V, \tag{2}$$

where $\mathbf{E}(t) = (E_x(t), 0, E_z(t))$ is the EP laser electric field, $E_x(t) = a(t)\frac{E_0\varepsilon}{\sqrt{1+\varepsilon^2}}\sin\omega t$, $E_z(t) = a(t)\frac{E_0}{\sqrt{1+\varepsilon^2}}\cos\omega t$, and E_0 is the amplitude. The envelope function $a(t)$ is defined by

$$a(t) = \begin{cases} \sin^2\left(\dfrac{\pi t}{6T}\right), & t \le 6T \\ 0, & t > 6T \end{cases}, \tag{3}$$

where T is the laser pulse optical period.

To solve Eq. (2), the initial conditions of the tunneled electron are necessary. In the parabolic coordinates, the Schrödinger equation for a H-like atom in a laser field can be expressed as[15]

$$\frac{\partial^2 \phi}{\partial \eta^2} + \left(-\frac{I_p}{2} + \frac{1}{2\eta} + \frac{1}{4\eta^2} + \frac{1}{4}E\eta\right)\phi = 0, \tag{4}$$

where I_p is the ionization potential. Therein, Eq. (4) describes a tunneling process for an electron with energy of $-\frac{1}{4}I_p$ within an effective potential of $U(\eta)$, i.e., $U(\eta)=-\frac{1}{4}I_p$, where $U(\eta)=-(\frac{1}{4\eta}+\frac{1}{8\eta^2}+\frac{1}{8}E\eta)$. Thus, the tunnel exit point η_0 can be determined by solving the equation of $-(\frac{1}{4\eta}+\frac{1}{8\eta^2}+\frac{1}{8}E\eta)=-\frac{I_p}{4}$.

In our calculation, the laser electric field is EP, which could be more complicated than the linearly polarized case. Following the procedure in Refs. [36,37], the EP laser field is assumed to be a rotating linearly polarized field. Thus, the initial conditions are obtained by introducing a rotating coordinate system, which are then projected to the laboratory frame. With this procedure, the initial positions of the tunnel ionized electron in the rotating frame are $x_0'=y_0'=0$ and $z_0'=-\frac{1}{2}\eta_0$. Correspondingly, the initial conditions in the laboratory frame are $x_0=-\frac{1}{2}\eta_0\sin\{\arctan[\varepsilon\tan(\omega t_0)]\}$, $y_0=0$, and $z_0=-\frac{1}{2}\eta_0\cos\{\arctan[\varepsilon\tan(\omega t_0)]\}$. The tunneled electron is assumed to have a zero initial longitudinal velocity and a nonzero initial transverse velocity with Gaussian distribution. Thus, the initial velocities are obtained by projecting the rotated coordinate into the original coordinate: $v_{x0}=v_{\rm per}\cos\theta\cos\{\arctan[\varepsilon\tan(\omega t_0)]\}$, $v_{y0}=v_{\rm per}\sin\theta$, and $v_{z0}=-v_{\rm per}\cos\theta\sin\{\arctan[\varepsilon\tan(\omega t_0)]\}$, where θ is the angle between $v_{\rm per}$ and the x' axis. The weight of each electron orbit is calculated by[30]

$$w(t_0,v_{\rm per})=w(0)\overline{w(1)},$$

$$w(0)=\frac{4(2I_p)^2}{|E|}\exp[-2(2I_p)^{\frac{3}{2}}/3|E|],$$

$$\overline{w(1)}=\frac{v_{\rm per}(2I_p)^{\frac{1}{2}}}{\pi|E|}\exp[-v_{\rm per}^2(2I_p)^{\frac{1}{2}}/|E|], \quad (5)$$

where t_0 is the tunneling moment, and $v_{\rm per}$ is the initial velocity.

In Fig. 1, the results for Ar calculated based on the simpleman model at 800 nm are presented. In the inset of Fig. 1(a), the EP laser electric field is graphically illustrated. The PMD for Ar subject to EP laser fields at the intensity of 3×10^{14} W/cm^2 and the ellipticity of 0.7 is depicted in Fig. 1(a). As shown in this panel, the PMD is concentrated on a thin curve, which deviates significantly from the typical measurements (see, e.g., Ref. [9]). The deviation can be attributed to the absence of the Coulomb potential and the initial photoelectron velocities when it is ionized by tunneling in our calculation. With closer inspection, the yields maxima appear at the minor axis of the polarization ellipse. This result can be comprehended with the fact that, based on the physical picture of the simpleman model, the photoelectron will be ionized through tunneling, most likely at the major axis of the polarization ellipse due to the local field strength maxima in those directions, and will eventually drift in a direction perpendicular to the instantaneous field from which it was released[38].

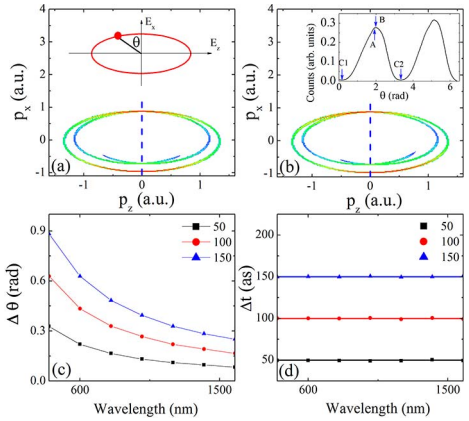

Fig. 1. (a) Calculated PMD for Ar, which is obtained with the simpleman model. The inset shows the sketch of the EP laser field. The wavelength is 800 nm, the ellipticity is 0.7, and the laser intensity is 3×10^{14} W/cm^2. (b) The calculated PMD with parameters identical to those of (a) except for the artificially introduced 100 as tunneling time delay. The inset picture is the corresponding photoelectron angular distribution. (c) Wavelength dependence of the offset angle calculated with the simpleman model, including the tunneling delay times of 50, 100, and 150 as, respectively. (d) The wavelength dependence of temporal offset Δt, which is extracted from the data in (c). See text for details.

To investigate the influence of tunneling delay of photoelectrons, an artificial time delay, δt, is introduced, i.e., rather than the instant right after tunneling at t_0, the photoelectron trajectory is launched at $t_0+\delta t$, before which the photoelectron stays at the origin. The calculated result with the parameters identical to those of Fig. 1(a), except for the delay of $\delta t=100$ as, is presented in Fig. 1(b). As shown, the PMD is rotated to some extent due to the time delay. With closer inspection, the asymmetry of the PMD can be identified in this panel, which becomes even more obvious in the angular distributions of photoelectrons in the inset of Fig. 1(b).

In a typical attoclock experiment, the angular deviation of yield maximum [indicated by B in the inset of Fig. 1(b)] from the simpleman model prediction[9] is usually employed to extract the tunneling delay time information. According to our calculation, due to the asymmetry of PMD, this procedure will give rise to an error of around 3.6 as. Here, we employ a more precise procedure. As shown in the inset of Fig. 1(b), there are two broad humps. The relevant angles of the first hump are indicated with A, B, C1, and C2, respectively. C1 and C2 indicate the left and right yield minima of the first hump, and A indicates the angle at which the photoelectron yields in the angular interval of [C1, A] equal that of [A, C2]. The error will become around 0.12 as if A (instead of B) is employed to extract the tunneling delay.

To demonstrate the advantage of our procedure and its physical origin, further numerical calculations have been carried out and presented in Fig. 2. In all the panels of this figure, A and B stand for the same meaning as those of the

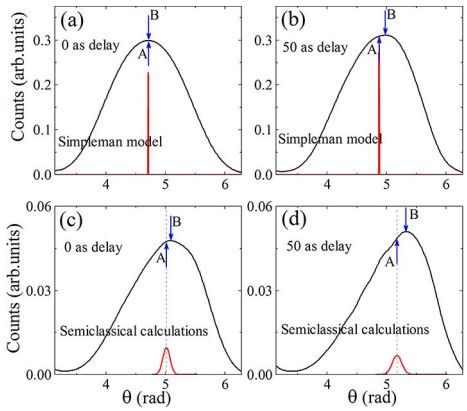

Fig. 2. Calculated photoelectron angular distributions for Ar subject to an EP laser field with ellipticity of $\varepsilon = 0.7$, based on the simpleman [(a) and (b)] and the semiclassical methods [(c) and (d)]. The tunneling delays are 0 as [(a) and (c)] and 50 as [(b) and (d)], respectively. The laser wavelength is 800 nm. The red lines indicate the angular distributions of photoelectron tunneling around the peak of the electric field envelope with a small interval of [3T-0.1 a.u., 3T+0.1 a.u.].

corresponding capital letters in the inset of Fig. 1(b). As shown in Fig. 2(a), A and B are consistent with each other for numerical calculations based on the simpleman model with zero tunneling delay. Note that the photoelectron trajectory with corresponding delay starting from the instant around the peak of the laser electric field has been indicated with the red line in each panel, which can be employed to show the correct angle corresponding to the instant of the peak laser electric field. On the other hand, when the tunneling delay is 50 as, even with the simpleman model, A and B show significant difference. Apparently, A instead of B, is the better choice. The difference between A and B can be attributed to the nonlinear correspondence between the measured angle and the emission instant, which becomes complicated when the effects of nonzero tunneling delay and Coulomb potential are included. Nevertheless, as shown in Figs. 2(b)–2(d), A can always be applied to find the correct angle.

To transfer the offset angle measured in an attoclock experiment to time delay, usually, the equation of $\Delta t = \Delta\theta/\omega_0$ is employed[8,9,18], which is accurate only when a perfect circularly polarized laser field is applied. In contrast, for an EP laser field, the laser electric field vector rotates with a variable angular frequency[39], and the relationship between the offset angle $\Delta\theta$ and the corresponding time delay Δt can be described by

$$\Delta t = \arctan(\varepsilon \tan \Delta\theta)/\omega_0, \tag{6}$$

where ε is the laser ellipticity. Equation (6) can be employed to obtain the delay information from the offset angle to improve the accuracy of the attoclock scheme.

With the two improvements discussed above, the tunneling delay can be obtained with high accuracy. In Fig. 1(c), the wavelength dependence of the angular offset achieved with the procedure described above is depicted for the time delay of 50, 100, and 150 as, respectively. The angular offset decreases smoothly as an exponential function of wavelength. With Eq. (6), the corresponding temporal offset can be obtained and is presented in Fig. 1(d), where all of the delay times are faithfully reproduced.

To further study the Coulomb potential influence, three-dimensional semiclassical calculations have been performed, where the Coulomb potential of the corresponding model atom is fully included. The typical PMD of Ar is presented in Fig. 3(a). With the procedure described above, the temporal offset with respect to the result of the simpleman model can be extracted accurately. The wavelength dependence of the temporal offset is depicted in Fig. 3(b). In contrast to the horizontal lines identified in Fig. 1(d), an obvious decreasing trend of the wavelength dependence of the extracted temporal offset can be obtained from the semiclassical calculations. Since the laser intensity is kept constant, according to the formula with quasi-static approximation (see, e.g., Ref. [12]), the tunnel exit is identical for the rising wavelength. Thus, the Coulomb potential strength experienced by the photoelectron at the tunnel exit is also identical. Nevertheless, the slope of the TOCP decreasing trend is abrupt at a shorter wavelength and becomes moderately smooth at a longer wavelength, indicating the complexity of the photoelectron dynamics in Coulomb potential. Here, it is assumed that the tunneling delay is constant with the rising wavelength due to the constant laser intensity. If this time of delay is further introduced, as shown in Fig. 3(b), the curve will be shifted up with the corresponding amount of time. From this result, we can understand that the

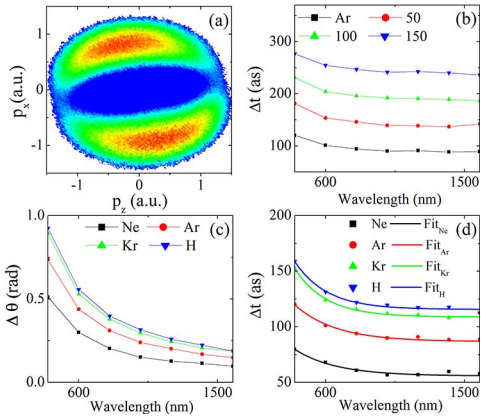

Fig. 3. (a) PMD for Ar calculated with the semiclassical model. The laser parameters are identical to those of Fig. 1(a). (b) Wavelength dependence of temporal offset extracted from the semiclassical calculations for Ar with the tunneling delay times of 0, 50, 100, and 150 as, respectively. (c) Wavelength dependence of the offset angle calculated with semiclassical model for both Ne and Ar, where no tunneling delay is included. (d) The corresponding wavelength dependence of the temporal offsets extracted from the data of Fig. 3(c) and their exponential fits. The difference between the fits for Ar and Ne is also shown in (d). See text for details.

Coulomb potential will induce a temporal offset sensitive to the wavelength, while the tunneling delay is insensitive to the wavelength if laser intensity is kept constant, which might be employed to extract the TOCP.

To shed more light on the relationship between the decreasing trend in Fig. 3(b) and the Coulomb potential influence, calculations for other model atoms of H, Kr, and Ne have also been performed and compared to those of Ar, where no further artificial tunnel delay is introduced. In our calculation, the strength of Coulomb potential is related to the ionization potential of the atom in question. For example, as is well known, the ionization potential of Ne is 21.56 eV, which is higher than that of Ar (15.76 eV). Hence, the deviation of the angular offset from that of Ar is expected for Ne. Indeed, in Fig. 3(c), where the wavelength dependence of the angular offset of Ne is compared to that of Ar, a significant difference between the results of the two atoms can be identified. With closer inspection, the angular offset is clearly larger for Ar. Although the Coulomb potential of Ne could be stronger than that of Ar, the main difference comes from the inner part around the nucleus in the spatial range of several atomic units. In the outer part, the difference of the Coulomb potential strength is not significant. On the other hand, the tunnel exit of Ne is larger than that of Ar[12]. Hence, the strength of the Coulomb potential at the tunnel exit experienced by the photoelectron of Ar is stronger than that of Ne, which gives rise to larger angular offset of Ar. Furthermore, as shown in Fig. 3(c), the deviation becomes smaller for longer wavelengths, indicating that the wavelength dependence of angular offset might be related to the strength of Coulomb potential. Similar analyses can be performed for other atoms. Therefore, the angular offset is larger for atoms with lower ionization potential, and this I_p dependence law is consistent with our calculations for all the model atoms.

In Fig. 3(d), the wavelength dependence of TOCP extracted with Eq. (6) is presented. The numerical calculations are shown with symbols, and the exponential fit curves are indicated with lines. As shown in Fig. 3(d), the temporal offset of each atom declines gradually with respect to wavelength. In the meantime, all of the atoms show a similar trend, and the wavelength dependence curves of the two with similar ionization potentials (e.g., H and Kr) are very close to each other. On the other hand, the curves deviate significantly for atoms with very different ionization potentials (e.g., Ar and Ne). This result gives us a hint that the wavelength dependence of TOCP might be related to the value of I_p of the atom in question.

In Fig. 4, the wavelength dependence of the ratios of TOCP of Ne, Ar, and Kr over that of H is presented. As shown in this figure, all of the data show the trend of horizontal lines. We fit the data of each atom with a horizontal line, and the obtained ratio is depicted with respect to the ionization potential in the inset, where the numerical calculation results closely follow the function of $(2I_p)^{-3/2}$. As already demonstrated numerically[18] and experimentally[19], Coulomb potential is the sole cause of the measured

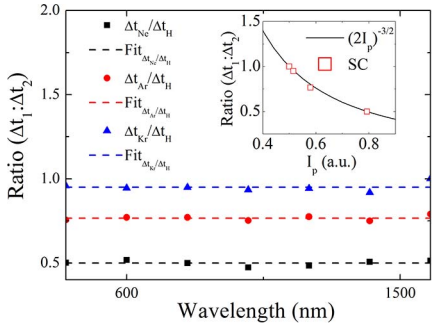

Fig. 4. Wavelength dependence of the ratios of TOCP of Ne, Ar, and Kr over that of H. The semiclassical calculation results are presented with symbols, and the horizontal line fit is shown with dashed lines. The ionization potential dependence of the ratio for each atom is depicted in the inset, where the semiclassical calculation (SC) result extracted by the fit procedure is shown with red open squares, and the function of $(2I_p)^{-3/2}$ is given with a black solid line.

offset angle for atom H. Therefore, with this result, the TOCP of any atom with a H-like potential, can be achieved easily with the given ionization potential.

With the attoclock experimental scheme, the results similar to the ones in Fig. 3(b) can be measured, except that, for a real experiment, the delay time is unknown and entangled with the TOCP. With a commercially available mid-infrared laser system, the wavelength dependence of the PMD can be measured, and the corresponding angular offset (and also the TOCP) can be further extracted. If the laser intensity is kept constant, and the wavelength is long enough to eliminate the non-adiabatic effect, the tunneling delay would only contribute a vertical shift of the whole curve, as shown in Fig. 3(b), which may not influence the slope of the wavelength dependence of the angular offset and also the TOCP. Thus, with the $(2I_p)^{-3/2}$ dependence law of the TOCP, we can extract the TOCP of the target atom with its relationship with that of H atom, for which the TOCP can be measured experimentally or calculated numerically with high accuracy.

In conclusion, the Coulomb potential effect of noble gas atoms subject to a strong EP laser field has been investigated with the semiclassical method. Based on our calculations, the $(2I_p)^{-3/2}$ dependence law of the TOCP has been revealed, and a procedure to experimentally extract the TOCP has been proposed for attoclock experiments. To optimize the temporal resolution of the attoclock technique, two improvements of the analysis procedure of the attoclock experimental data have been described. Our work is significant for the accurate measurement of the tunneling delay in the tunneling ionization of atoms subject to an intense EP laser field.

This work is supported by the National Key Research and Development Program of China (Nos. 2019YFA0307702, 2019YFA0307704, and 2016YFA0401100), the National Natural Science Foundation of China (Nos. 11974383,

11834015, 11847243, 11804374, 11874392, 11774387, 11527807, and 11425414), and the Strategic Priority Research Program of the Chinese Academy of Sciences (No. XDB21010400).

References

1. J. Du and T. Kobayshi, Chin. Opt. Lett. **9**, S10601 (2011).
2. H. Xie, G. Li, J. Yao, W. Chu, Z. Chen, and Y. Cheng, Chin. Opt. Lett. **16**, 120201 (2018).
3. L. A. MacColl, Phys. Rev. **40**, 621 (1932).
4. M. Hentschel, R. Kienberger, Ch. Spielmann, G. A. Reider, N. Milosevic, T. Brabec, P. Corkum, U. Heinzmann, M. Drescher, and F. Krausz, Nature **414**, 509 (2001).
5. R. Kienberger, E. Goulielmakis, M. Uiberacker, A. Baltuska, V. Yakovlev, F. Bammer, A. Scrinzi, Th. Westerwalbesloh, U. Kleineberg, U. Heinzmann, M. Drescher, and F. Krausz, Nature **427**, 817 (2004).
6. P. M. Paul, E. S. Toma, P. Breger, G. Mullot, F. Augé, Ph. Balcou, H. G. Muller, and P. Agostini, Science **292**, 1689 (2001).
7. Y. Mairesse, A. de Bohan, L. J. Frasinski, H. Merdji, L. C. Dinu, P. Monchicourt, P. Breger, M. Kovačev, R. Taïeb, B. Carré, H. G. Muller, P. Agostini, and P. Salières, Science **302**, 1540 (2003).
8. P. Eckle, M. Smolarski, P. Schlup, J. Biegert, A. Staudte, M. Schöfler, H. G. Muller, R. Döner, and U. Keller, Nat. Phys. **4**, 565 (2008).
9. P. Eckle, A. N. Pfeiffer, C. Cirelli, A. Staudte, R. Dörner, H. G. Muller, M. Büttiker, and U. Keller, Science **322**, 1525 (2008).
10. K. J. Schafer, B. Yang, L. F. DiMauro, and K. C. Kulander, Phys. Rev. Lett. **70**, 1599 (1993).
11. P. B. Corkum, Phys. Rev. Lett. **71**, 1994 (1993).
12. A. S. Landsman and U. Keller, Phys. Rep. **547**, 1 (2015).
13. H. Ni, N. Eicke, C. Ruiz, J. Cai, F. Oppermann, N. I. Shvetsov-Shilovski, and L.-W. Pi, Phys. Rev. A **98**, 013411 (2018).
14. R. Xu, T. Liu, and X. Wang, Phys. Rev. A **98**, 053435 (2018).
15. I. A. Ivanov, A. S. Kheifets, J. E. Calvert, S. Goodall, X. Wang, H. Xu, A. J. Palmer, D. Kielpinski, I. V. Litvinyuk, and R. T. Sang, Sci. Rep. **6**, 19002 (2016).
16. J. Liang, R. Zhang, X. Ma, Y. Zhou, and P. Lu, Chin. Opt. Lett. **16**, 040202 (2018).
17. A. N. Pfeiffer, C. Cirelli, M. Smolarski, D. Dimitrovski, M. Abu-samha, L. B. Madsen, and U. Keller, Nat. Phys. **8**, 76 (2012).
18. L. Torlina, F. Morales, J. Kaushal, I. Ivanov, A. Kheifets, A. Zielinski, A. Scrinzi, H. G. Muller, S. Sukiasyan, M. Ivanov, and O. Smirnova, Nat. Phys. **11**, 503 (2015).
19. U. S. Sainadeh, H. Xu, X. Wang, A. Atia-Tul-Noor, W. C. Wallace, N. Douguest, A. Bray, I. Ivanov, K. Bartschat, A. Kheifets, R. T. Sang, and I. V. Litvinyuk, Nature **568**, 75 (2019).
20. A. S. Landsman, M. Weger, J. Maurer, R. Boge, A. Ludwig, S. Heuser, C. Cirelli, L. Gallmann, and U. Keller, Optica **1**, 343 (2014).
21. N. Camus, E. Yakaboylu, L. Fechner, M. Klaiber, M. Laux, Y. Mi, K. Z. Hatsagortsyan, T. Pfeifer, C. H. Keitel, and R. Moshammer, Phys. Rev. Lett. **119**, 023201 (2017).
22. E. Yakaboylu, M. Klaiber, and K. Z. Hatsagortsyan, Phys. Rev. A **90**, 012116 (2014).
23. A. W. Bray, S. Eckart, and A. S. Kheifets, Phys. Rev. Lett. **121**, 123201 (2018).
24. M. Klaiber, E. Yakaboylu, H. Bauke, K. Z. Hatsagortsyan, and C. H. Keitel, Phys. Rev. Lett. **110**, 153004 (2013).
25. T. Zimmermann, S. Mishra, B. R. Doran, D. F. Gordon, and A. S. Landsman, Phys. Rev. Lett. **116**, 233603 (2016).
26. L. Guo, M. Liu, R. Lu, S. Han, and J. Chen, *Laser and Particle Beams* (Cambridge University, 2019), p. 1.
27. G. G. Paulus, W. Becker, W. Nicklich, and H. Walther, J. Phys. B **27**, L703 (1994).
28. M. V. Ammosov, N. B. Delone, and V. P. Krainov, Sov. Phys. JETP **64**, 1191 (1986).
29. B. Hu, J. Liu, and S.-G. Chen, Phys. Lett. A **236**, 533 (1997).
30. N. B. Delone and V. P. Krainov, J. Opt. Soc. Am. B **8**, 1207 (1991).
31. T. Brabec, M. Y. Ivanov, and P. B. Corkum, Phys. Rev. A **54**, R2551 (1996).
32. J. Chen, J. Liu, L. B. Fu, and W. M. Zheng, Phys. Rev. A **63**, 011404 (R) (2000).
33. L. B. Fu, J. Liu, J. Chen, and S. G. Chen, Phys. Rev. A **63**, 043416 (2001).
34. J. Chen, J. Liu, and W. M. Zheng, Phys. Rev. A **66**, 043410 (2002).
35. D. F. Ye, X. Liu, and J. Liu, Phys. Rev. Lett. **101**, 233003 (2008).
36. X. L. Hao, G. Q. Wang, X. Y. Jia, W. D. Li, J. Liu, and J. Chen, Phys. Rev. A **80**, 023408 (2009).
37. M. Y. Wu, Y. L. Wang, X. J. Liu, W. D. Li, X. L. Hao, and J. Chen, Phys. Rev. A **87**, 013431 (2013).
38. P. B. Corkum, N. H. Burnett, and F. Brunel, Phys. Rev. Lett. **62**, 1259 (1989).
39. C. Hofmann, A. S. Landsman, and U. Keller, J. Mod. Opt. **66**, 1052 (2019).